Energy Equip. Sys./ Vol. 13/No. 3/September 2025/ 193-209

ENERGY EQUIPSYS

Energy Equipment and Systems

www.energyequipsys.com

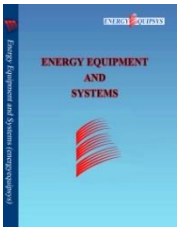

3E analysis and multi-criteria optimization of a Salinity Gradient Solar Pond (SGSP) integrated power plant

Manuscript Type
Research Paper

Authors

Joy Nondy [a*]

[a] Department of Sustainable Energy Engineering, Indian Institute of Technology Kanpur, Uttar Pradesh, 208016, India

Article history:
Received: 10 December 2024
Revised: 14 April 2025
Accepted : 28 April 2025

ABSTRACT

This study introduces a novel salinity gradient solar pond (SGSP)-integrated power plant that combines a recuperative-regenerative organic Rankine cycle (RR-ORC) and a thermoelectric generator (TEG) for efficient low-temperature power generation. The RR-ORC, featuring an internal heat exchanger and a feed heater, is selected for its superior thermodynamic and economic performance compared to conventional ORC configurations. A comprehensive energy, exergy, and exergoeconomic (3E) analysis is performed, followed by multi-criteria optimization using NSGA-II and TOPSIS to enhance exergy efficiency while minimizing system costs. The results indicate that under optimal operating conditions, the system delivers a power output of 1987 kW, with energy and exergy efficiencies of 10.3% and 14.36%, respectively, and a system cost rate of $182.94 per hour. This study underscores the potential of solar pond-based power plants as a sustainable and cost-effective solution for renewable energy generation.

Keywords: Salinity Gradient, NSGA-II, Solar Pond, Thermoelectric Generator, ORC.

1. Introduction

With the depletion of fossil fuels and the environmental challenges they pose, scientists are increasingly exploring alternative energy sources that can sustainably meet humanity's energy needs. Renewable energy, particularly solar energy, stands out as a plentiful and inexhaustible resource. Among the various solutions proposed for harnessing solar energy, salinity gradient solar ponds (SGSPs) have emerged as a promising option that offers the dual benefits of energy storage and serving as a heat source for low-temperature cycles. Salts such as magnesium chloride, sodium chloride, or sodium nitrite dissolve in water, creating a salinity gradient with concentrations ranging from 30% at the bottom to 20% at the surface. This gradient results in the formation of three separate layers within the pond: the upper convective zone (UCZ), the non-convective zone (NCZ), and the lower convective zone (LCZ). The UCZ and LCZ are homogeneous, with heat transfer occurring predominantly within these convective zones [1]. The LCZ, containing saturated brine with nearly uniform salinity and density, serves as the primary energy storage layer [2]. SGSPs are effective systems for harnessing solar energy for power generation, desalination, and industrial heating applications. Recent advancements focus on improving the efficiency of SGSPs through hybrid system integration [3].

Khalilian [4] conducted both experimental and numerical studies on a square solar pond with an area of 4 m² and a height of 1.1 m. His

* Corresponding author: Joy Nondy
Department of Sustainable Energy Engineering, Indian Institute of Technology Kanpur, Uttar Pradesh, India
Email: joynondy21.jn@gmail.com

research also included modeling the effects of sidewall shadows. The findings revealed that the energy efficiency was 3.27% with shadow effects and 3.65% without them. In another study, El Mansouri et al. [5] performed transient modeling of three heat exchangers for an SGSP using exergy analysis. Their results identified the vertical heat extraction technique as the most efficient method for heat transfer from the UCZ in terms of both energy and exergy efficiency.

A wide range of studies have explored various aspects of salinity SGSPs, each focusing on specific characteristics of these systems. Babaei et al. [6] analyzed the use of spiral pipes with different flat axes to enhance solar pond performance. Similar investigations have been conducted by Dehghan et al. [7] Njoku et al. [8] and Faqeha et al. [9]. In recent years, there has been significant interest in integrating solar ponds with low-temperature thermodynamic cycles, leading to extensive research in this area. In a study, Ziapour et al. [10] proposed a solar pond-based power plant utilizing solar ponds as the heat source to drive a basic ORC. Instead of a conventional condenser, they integrated a TEG into the system. The results showed that the thermal efficiency of the proposed power plant was 0.21% higher compared to the system without the thermoelectric generator.

Damarseckin et al.[11] investigated an SGSP integrated with parabolic trough collectors for electricity and hydrogen generation. The system, incorporating an ORC with n-butane, utilizes waste heat for heating and preheated water to enhance ORC performance. Analyzing five mass flow rates, they found that lower flow rates improve efficiency, with peak hydrogen production reaching 534.32 g/day. The system's maximum energy and exergy efficiencies were reported as 13.77% and 5.79%, respectively. Musharavati et al.[12] proposed a hybrid system combining an SGSP with a proton exchange membrane fuel cell (PEMFC) and a TEG for efficient energy utilization. The PEMFC's waste heat enhances the solar pond's performance, while the TEG maximizes waste energy recovery. Under base conditions, the system achieves a net output of 2288.8 kW with energy and exergy efficiencies of 11.26% and 13.17%, respectively. Optimization further enhances performance by over 50% with a minimal cost increase, highlighting the system's potential for improved energy efficiency and sustainability.

Zeynali et al. [13] investigated a modified ORC and a modified trilateral flash cycle (TFC) coupled with a SGSP. Their results revealed that the maximum power generation occurred at mass flow rates of 0.1082 kg/s for the ORC and 0.1224 kg/s for the TFC. Musaffa and Farshi [14] evaluated the feasibility of an SGSP-based power system employing an ORC with a two-pressure level and a zeotropic working fluid. The system also utilized the cooling potential of liquefied natural gas as a sink and showed an efficiency of 20%.

Various studies on solar ponds have demonstrated the potential to integrate different thermodynamic systems to generate useful energy products. Parsa et al.[15] conducted a comprehensive thermodynamic and economic analysis of an SGSP-based multi-effect desalination system. Their findings demonstrated that the proposed system could produce 20,000 tons of fresh water annually, with an estimated payback period of six years. In another study, Manzoor et al. [16] examine the incorporation of an SGSP with a direct contact membrane distillation system under the climatic conditions of Islamabad. The SGSP, with a surface area of 4.65 m^2, served as a heat source to pre-warm brine for temperature-driven desalination processes. Their findings revealed that the DCMD system's performance improved with greater temperature differentials, achieving stable permeate flux and high salt rejection, thereby highlighting the potential of SGSP-extracted heat for efficient desalination applications. El Mansouri et al. [17] present a solar desalination system powered entirely by solar energy, integrating an SGSP with an ORC to drive reverse osmosis pumps. Through theoretical modelling and genetic algorithm optimization, the system achieves a specific energy consumption of 2.1 kWh/m^3 and an exergy efficiency of 54% with a daily drinking water production capacity of 2380.8 m^3.

Several studies have explored the technical and economic aspects of SGSP-based hybrid systems. Li et al. [18] conducted a comparative study on the performance of an SGSP for hydrogen production using two thermodynamic cycles: an absorption power cycle and an organic Rankine cycle (ORC) with a zeotropic

mixture. Through exergoeconomic analysis, they found that the ORC outperformed the APC, achieving higher energy (5.86%) and exergy efficiency (29.48%) while reducing the unit cost of the product to 47.27 $/GJ. Zoghi et al. [19] conducted a comparative study of three renewable energy systems—wind turbine, SGSP, and ocean thermal energy conversion—for hydrogen production using an exergoeconomic approach. These systems are integrated with a trilateral cycle and a TEG for heat recovery, with hydrogen generated by a PEM electrolyzer. The results show that the wind-based system achieves the highest exergy efficiency (5.8–10.47%) and the lowest total cost rate (66.08 $/h), while the SGSP-based system is the most economical for hydrogen production, with a unit cost ranging from 42.78 to 44.31 $/GJ.

Based on the reviewed literature, it is evident that while SGSPs have been integrated with basic ORCs and other low-temperature thermodynamic systems, the combination of an SGSP with an RR-ORC and a TEG remains unexplored. This study proposes a novel integrated configuration in which the SGSP serves as the primary heat source for a hybrid RR-ORC/TEG system. The RR-ORC, incorporating both a recuperator and a feed heater, enables enhanced internal heat recovery, leading to improved thermal efficiency over conventional ORC layouts [20]. In parallel, the TEG module utilizes the temperature difference between the hot brine exiting the vapour generator and cooling water from an external circuit to generate direct current electricity, offering an additional energy recovery pathway. Furthermore, unlike previous studies that typically emphasize either thermodynamic or economic performance, this work presents comprehensive energy, exergy, and exergoeconomic analysis of the proposed system. Moreover, key design parameters are optimized to enhance efficiency and cost-effectiveness. These innovations highlight the unique potential of the proposed system as an efficient, multi-output solution for sustainable energy conversion using solar ponds.

The objectives of the present research are listed as follows:

- Introducing a novel solar pond-based system integrating RR-ORC and thermoelectric modules to generate power.
- Conducting energy, exergy, and exergoeconomic (3E) analyses to determine the system's cost rate.
- Performing a parametric analysis of critical operating conditions.

Implementing multi-criteria optimization to improve thermodynamic performance and reduce system cost rate.

2. System description

Figure 1presents the schematic representation of the SGSP integrated power plant. This setup combines an RR-ORC with a TEG. The RR-ORC includes key components such as a Vapor Turbine (VT), Internal Heat Exchanger (IHE), Feed Heater (FH), Condenser (COND), Vapor Generator (VG), and Feed Pumps (FP-II and FP-III). The cycle begins with hot brine exiting the SGSP at State 1, which FP-I then pressurizes to State 2 before entering the VG. Within the VG, the thermal energy of the brine is transferred to the organic working fluid (R123), causing it to evaporate into high-pressure vapor at State 7. The now-cooled brine exits the VG at State 3 and is directed toward the TEG. The high-pressure vapor expands in the VT to an intermediate pressure at State 8, where a portion is diverted to pre-warm the working fluid in the FH. The remaining vapor continues to expand to a lower pressure at State 9. This low-pressure vapor then flows through the IHE, where it transfers residual heat to the subcooled liquid working fluid before entering the COND at State 10. The external cooling circuit for the condenser is represented by States 16–17. The condensed liquid exits the condenser at State 11 and is subsequently pressurized by Feed Pump II (FP-II) to State 12. It is then pre-warmed in the IHE and blended with the separated vapor in the FH at State 13. This combined stream is further pressurized by Feed Pump III (FP-III) to State 15 and returned to the vapor generator, thus completing the cycle. Simultaneously, the TEG utilizes the temperature gradient between the cooled brine at State 3 and an external cooling water circuit (States 5–6) to produce additional electricity.

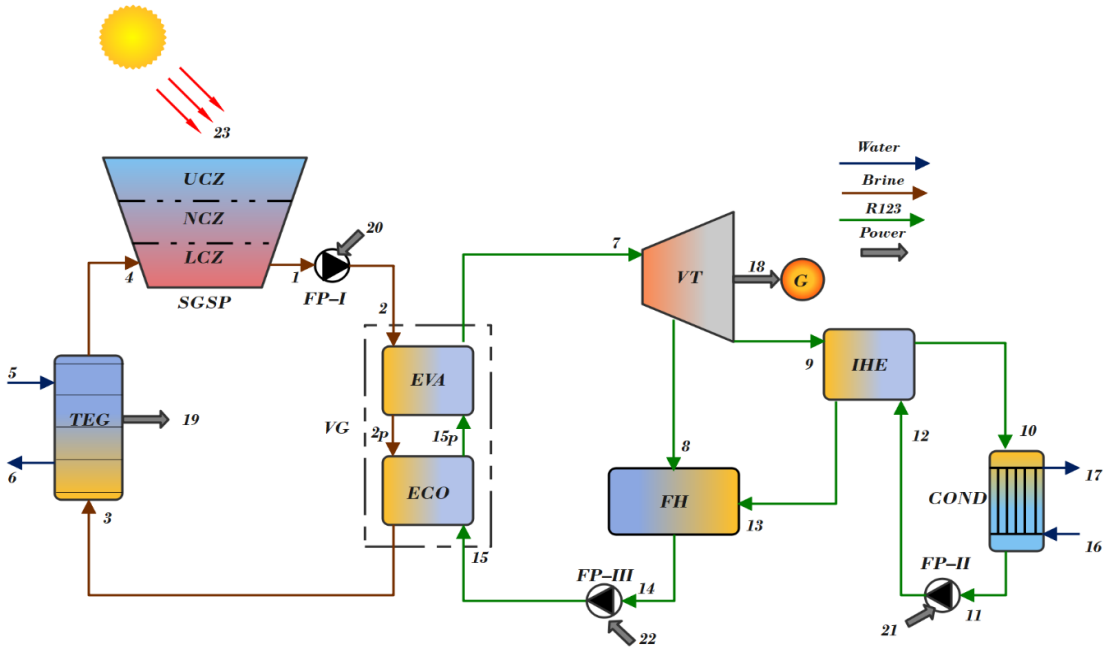

Fig. 1. Layout of the SGSP integrated power plant.

3. Modelling

This part of the study begins by stating the key premises considered for conducting the simulation. It then presents the fundamental equations and analytical methods employed for assessing the system's energy performance. Additionally, it covers the formulation of exergy and exergoeconomic models and explains the strategy adopted for conducting a multi-criteria optimization.

3.1 Input parameters

Tables 1 and 2 comprise control variables for simulating the proposed SGSP integrated power plant.

3.2 Energy and exergy analyses

The governing equations used for performing the energy analysis of the SGSP integrated plant are presented as follows [25]:

$$\sum \dot{m}_i - \sum \dot{m}_o = 0 \tag{1}$$

$$\sum (\dot{m}h)_i - \sum (\dot{m}h)_o + \left(\sum \dot{Q}_i - \sum \dot{Q}_o\right) + \dot{W} = 0 \tag{2}$$

To determine the exergy destruction rate of the proposed system, the exergy destruction rate of each individual component is first calculated using the exergy balance equation outlined in Eq. (3). Subsequently, the exergy destruction rates of all components are summed to obtain the total exergy destruction rate for the entire system[26].

Table 1. The control variables of the SGSP [21,22].

Parameters	Value	Unit
LCZ temperature	359.15-369.15	K
UCZ temperature	298.15	K
UCZ thickness	0.3	m
NCZ thickness	1	m
LCZ thickness	1.2	m
Pond surface area	100000	m^2
Solar radiation	800	W/m^2
UCZ's salinity	5	%
LCZ's salinity	25	%

Table 2. The control variables of the RR-ORC and TEG [23,24].

Parameters	Value	Unit
Turbine isentropic efficiency	80	%
Pump isentropic efficiency	85	%
Working medium	R123	–
VG outlet temperature	330-350	K
Condenser outlet temperature	300-308	K
Effectiveness of IHX	65	%
PPTD	5	K
Inlet water temperature of COND	298.15	K
Inlet water temperature of COND	303.15	K
Figure of merit	0.2-1.6	–
Thermoelectric material	BiCuSeO	–
Inlet condensate temperature	298.15	K
Outlet condensate temperature	303.15	K
Mass flow rate of R123	10-50	m/s

$$\dot{E}_{F,k} = \dot{E}_{P,k} + \dot{E}_{L,k} + \dot{E}_{D,k} \quad (3)$$

The exergy flow rate is evaluated by using Eq. (4).

$$\dot{E} = \dot{m}[(h - h_0) - T_0(h - s_0)] \quad (4)$$

The exergy balance equations for the system elements of the SGSP integrated plant are listed in Table 3.

3.3.Exergoeconomic analysis

The exergoeconomic analysis in this research employs the specific exergy costing (SEPCO) approach [28,29]. The cost rate is determined using Eq. (5) [30]:

$$\sum_{o} \dot{C}_{o,k} + \dot{C}_{work,k} = \dot{C}_{heat,k} + \sum_{i} \dot{C}_{i,k} + \dot{Z}_k \quad (5)$$

where, $\dot{C}$ is the cost flow rate in $\$/h$ and $\dot{Z}_k$ is the capital cost rate of the k^{th} component which is further calculated using the following relation [31]:

$$\dot{Z}_k = \frac{PEC_k \times CRF \times \phi}{N} \quad (6)$$

where, PEC_k is the purchase equipment cost, which is calculated by using the relations given in Table 4, N is the yearly operating hours (7446 hours), ϕ is the maintenance factor (1.06) [32] and CRF is the capital recovery factor, which is calculated by using Eq. (7) [33]:

$$CRF = \frac{j \times (1+j)^n}{(1+j)^n - 1} \quad (7)$$

where, j represents the interest rate (12%) and n denotes the operating life of the plant (20 years) [28].

Table 3. The energy and exergy relations used for modelling.

System elements	Energy balance equations	Exergy balance equations
SGSP	$\dot{Q}_{lu} = \dot{Q}_{lr} - \dot{Q}_{lt}$	$\dot{E}_4 + \dot{E}_{23} = \dot{E}_1 + \dot{E}_{D,SGSP-I}$
FP-I	$\dot{W}_{FP-I} = \dot{m}_s(h_2 - h_1)$	$\dot{E}_1 + \dot{E}_{20} = \dot{E}_2 + \dot{E}_{D,FP-I}$
FP-II	$\dot{W}_{FP-II} = \dot{m}_{r2}(h_{12} - h_{11})$	$\dot{E}_{11} + \dot{E}_{21} = \dot{E}_{12} + \dot{E}_{D,FP-II}$
FP-III	$\dot{W}_{FP-III} = \dot{m}_r(h_{15} - h_{14})$	$\dot{E}_{14} + \dot{E}_{22} = \dot{E}_{15} + \dot{E}_{D,FP-III}$
VG	$\dot{m}_s(h_2 - h_3) = \dot{m}_r(h_7 - h_{15})$	$\dot{E}_2 + \dot{E}_{15} = \dot{E}_7 + \dot{E}_3 + \dot{E}_{D,VG}$
TEG	$\dot{m}_s(h_3 - h_4) = \dot{m}_w(h_6 - h_5)$	$\dot{E}_3 + \dot{E}_5 = \dot{E}_6 + \dot{E}_4 + \dot{E}_{19} + \dot{E}_{D,TEG}$
VT	$\dot{W}_{VT} = \dot{m}_r(h_7 - h_8) + \dot{m}_{r2}(h_8 - h_9)$	$\dot{E}_7 = \dot{E}_8 + \dot{E}_9 + \dot{E}_{18} + \dot{E}_{20} + \dot{E}_{21} + \dot{E}_{22} + \dot{E}_{D,VT}$
IHE	$(h_9 - h_{10}) = (h_{13} - h_{12})$	$\dot{E}_9 + \dot{E}_{12} = \dot{E}_{10} + \dot{E}_{13} + \dot{E}_{D,IHE}$
COND	$\dot{m}_{r2}(h_{10} - h_{11}) = \dot{m}_w(h_{17} - h_{16})$	$\dot{E}_{10} + \dot{E}_{16} = \dot{E}_{11} + \dot{E}_{17} + \dot{E}_{D,COND}$
Overall system	$\eta_{tot} = \frac{\dot{W}_{net,ORC} + \dot{W}_{TEG}}{\dot{Q}_{lu}}$	$\epsilon_{tot} = \frac{\dot{W}_{net,ORC} + \dot{W}_{TEG}}{\dot{E}_{23}}$

The annual net cash flow (CF) of the system is calculated using Eq. (8) [34].

$$CF = Y_{el}K_{el} - K_{om} \tag{8}$$

where Y_{el} is the net generated electricity, K_{el} is the electricity expenses (0.22 $/kWh) [35] and K_{om} is the operation and maintenance expenses (= 6% of $\dot{Z}_{total}$[34]).

Further, the overall expenditure (C_o) is evaluated based on Ref. [29]. Further, the relations for evaluating the simple payback period (SPP) [29] and payback period (PP) [36] are given in Eqs. (9) and (10), respectively.

$$SPP = \frac{C_o}{ANCF} \tag{9}$$

$$PP = \frac{\ln\left(\frac{CF}{CF - r \times C_o}\right)}{\ln(1+r)} \tag{10}$$

where $\boldsymbol{r}$ denotes the discount rate (3%) [36]. The cost balance equations are listed in Table 4.

3.4. Multi-objective optimization

Multi-objective optimization refers to the process of optimizing more than one objective function simultaneously based on a defined set of decision variables. Instead of a single optimal point, this method generates a collection of trade-off solutions, collectively forming the Pareto frontier in a bi-objective space [38]. The mathematical expression of the multi-objective optimization problem tailored for the SGSP-based integrated system is provided in Eq. (11) [39].

$$\left.\begin{aligned} & x = (T_{LCZ}.\dot{m}_r.T_7.ZT_m)^T \\ & f = \left(f_1(\varepsilon_{tot}).f_2(\dot{C}_{sys})\right)^T \\ & g_j(x) \le 0 \;\; ; \quad \forall j = 1.2. \ldots \ldots j \\ & 359.15\ \text{K} \le T_{LCZ} \le\ 369.15\ \text{K} \\ & 10\ \text{m/s} \le \dot{m}_r \le\ 50\ \text{m/s} \\ & 330\ \text{K} \le T_7 \le\ 350\ \text{K} \\ & 0.2\ \le ZT_m \le 1.6 \end{aligned}\right\} \tag{11}$$

As seen in Eq. (11), the optimization framework employs four decision variables for the analysis of the proposed setup, namely:

- LCZ temperature ($\boldsymbol{T_{LCZ}}$)
- Mass flow rate of the R123 ($\boldsymbol{\dot{m}_r}$)
- Inlet temperature of the VT ($\boldsymbol{T_7}$)
- Figure of merit of the TEG ($\boldsymbol{ZT_m}$)

Table 4. The cost balance equations and purchase equipment costs [12,20,37]

Components	Cost balance equations	$\boldsymbol{PEC_k}$
SGSP	$\dot{C}_4 + \dot{C}_{23} + \dot{Z}_{SGSP} = \dot{C}_1$	$35 \times A_{pond}$
	$\dot{C}_{23} = 3600 \times \dot{m}_s \times 0.04$	
FP-I	$\dot{C}_1 + \dot{C}_{20} + \dot{Z}_{FP-II} = \dot{C}_2$	$3540 \times \dot{W}_{FP-I}^{0.71}$
FP-II	$\dot{C}_{11} + \dot{C}_{21} + \dot{Z}_{FP-II} = \dot{C}_{12}$	$3540 \times \dot{W}_{FP-II}^{0.71}$
FP-III	$\dot{C}_{14} + \dot{C}_{22} + \dot{Z}_{FP-II} = \dot{C}_{15}$	$3540 \times \dot{W}_{FP-III}^{0.71}$
VG	$\dot{C}_2 + \dot{C}_{15} + \dot{Z}_{VG} = \dot{C}_3 + \dot{C}_7$	$309.143 \times A_{VG} + 231.915$
	$\dot{C}_2\,\dot{E}_3 = \dot{C}_3\,\dot{E}_2$	
TEG	$\dot{C}_3 + \dot{C}_5 + \dot{Z}_{TEG} = \dot{C}_4 + \dot{C}_6 + \dot{C}_{19}$	$1500 \times \dot{W}_{TEG}$
	$\dot{C}_4\,\dot{E}_3 = \dot{C}_3\,\dot{E}_4$	
	$\frac{(\dot{C}_4 - \dot{C}_3)}{(\dot{E}_4 - \dot{E}_3)} = \frac{(\dot{C}_6 - \dot{C}_5)}{(\dot{E}_6 - \dot{E}_5)}$	
	$\dot{C}_5 = 0$	
VT	$\dot{C}_7 + \dot{Z}_{VT} = \dot{C}_8 + \dot{C}_9 + \dot{C}_{18} + \dot{C}_{20} + \dot{C}_{21} + \dot{C}_{22}$	$6000 \times \dot{W}_{VT}^{0.70}$
	$\dot{C}_7\,\dot{E}_8 = \dot{C}_8\,\dot{E}_7$	
	$\dot{C}_7\,\dot{E}_9 = \dot{C}_9\,\dot{E}_7$	
	$\dot{C}_{18}\,\dot{E}_{20} = \dot{C}_{20}\,\dot{E}_{18}$	
	$\dot{C}_{18}\,\dot{E}_{21} = \dot{C}_{21}\,\dot{E}_{18}$	
	$\dot{C}_{18}\,\dot{E}_{22} = \dot{C}_{22}\,\dot{E}_{18}$	
IHE	$\dot{C}_9 + \dot{C}_{12} + \dot{Z}_{IHE} = \dot{C}_{13} + \dot{C}_{10}$	$1.3(190 + 310 \times A_{IHE})$
	$\dot{C}_9\,\dot{E}_{10} = \dot{C}_{10}\,\dot{E}_9$	
COND	$\dot{C}_{10} + \dot{C}_{16} + \dot{Z}_{COND} = \dot{C}_{17} + \dot{C}_{11}$	$1773 \times \dot{m}_{r2}$
	$\dot{C}_{10}\,\dot{E}_{11} = \dot{C}_{11}\,\dot{E}_{10}$	
	$\dot{C}_{16} = 0$	

The bounds assigned to the decision variables, as outlined in Eq. (11), are established based on Ref. [12]. In this study, the chosen objective functions are the overall exergy efficiency (ε_{tot}) and the system cost rate ($\dot{C}_{sys}$). The optimization aims to enhance exergy performance while simultaneously reducing the system's cost rate. These objective functions are mathematically defined in Eqs. (12) [40] and (13) [41], respectively

$$\varepsilon_{tot} = \frac{\dot{W}_{net,ORC} + \dot{W}_{TEG}}{\dot{E}_{23}} \quad (12)$$

$$\dot{C}_{sys} = \dot{C}_{fuel} + \sum_{k} \dot{Z}_k + \sum_{k} \dot{C}_{D,k} + \dot{C}_L \quad (13)$$

where $\dot{C}_{fuel}$ denotes the fuel expenses and $\dot{C}_L$ denotes exergy loss cost.

To perform the multi-objective optimization of the SGSP integrated plant, the NSGA-II [42] has been utilized. For selecting the most suitable solution from the generated Pareto front, the Entropy-TOPSIS decision-making approach [44] is applied. The acronym TOPSIS [43] stands for Technique for Order Preference by Similarity to Ideal Solution. A comprehensive explanation of the TOPSIS methodology is available in Ref. [45], while the Entropy method is elaborated in Ref. [46].

4. Results and discussions

4.1. Validation

The SGSP model formulated in this study is verified through a comparative analysis with the model developed by Tsilingiris [47]. Figure 2 presents the relationship between pond efficiency and the NCZ depth, assuming a constant temperature of 60°C. The LCZ and UCZ were assigned depths of 0.8 m and 0.1 m, respectively, with the solar pond area set at 100,000 m². It is worth mentioning that in Ref. [47], Simulation results were based on daily solar radiation data recorded over three years. In contrast, the present study employs the average solar radiation value from that same period (200 W/m²), aligning with the steady-state assumptions of the model. As a result, minor discrepancies are noticeable, especially around the peak regions of the curves. Similar observations were made by Ziapour et al. [48], whose work also relied on steady-state simulation conditions. Additionally, the RR-ORC model has been verified by comparing the outputs with Ref. [49] for an identical RR-ORC configuration. Table 5 presents this comparison, demonstrating that the present model produces outputs closely aligned with Ref. [49]. Lastly, the TEG model was previously validated by the author in an earlier publication [12]; therefore, this validation is not repeated here.

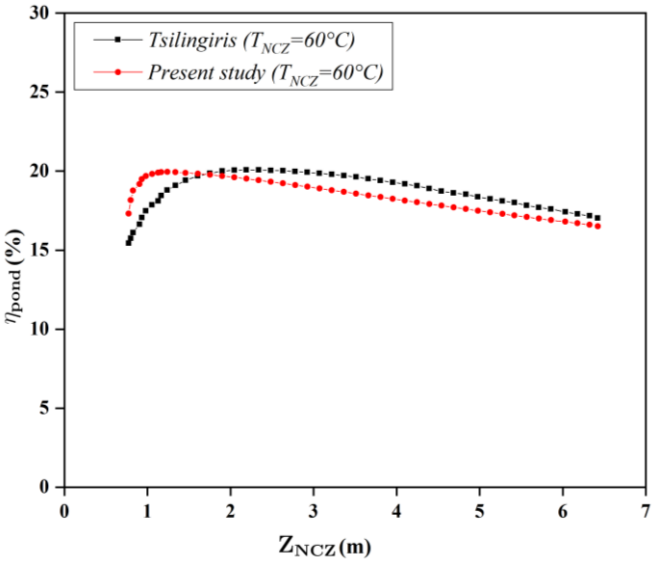

Fig. 2. Validation of SGSP model with Ref. [47].

Table 5. Validation of RR-ORC model with Ref. [50]

(P_{VG}=25 bar, P_{COND}=1 bar, P_{REG}=10 bar, $\dot{Q}_{VG}$=252 MW, $\eta_{s,T}$=80%,$\eta_{s,P}$=85%)

Parameters	Ref. [50]	Present work	Error (%)
$\dot{W}_{net}$ (kW)	57.54	58.84	2.25
η_{sys} (%)	22.83	23.3	2.05
$\dot{E}_D$ (kW)	42.2	43.2	2.36

4.2 Parametric analysis

The parametric analysis is conducted by individually varying critical operating conditions and observing the effects on total power output ($\dot{W}_{tot}$), energy efficiency (η_{tot}), exergy efficiency (ε_{tot}) and system cost rate ($\dot{C}_{sys}$). The critical operating conditions selected for conducting the parametric analysis are the temperature of the low conductive zone (T_{LCZ}), the figure of merit (ZT_m), VT inlet temperature (T_7), condenser temperature (T_{11}) and the mass flow rate of R123 ($\dot{m}_r$). Figure 3 shows that when T_{LCZ} rises, $\dot{W}_{tot}$, η_{tot} and ε_{tot} fall due to a drop in the usable heat removal rate from the SGSP. It can also be observed that $\dot{C}_{sys}$ also reduces mostly because of rise in exergy destruction cost. It is noteworthy that, as a performance metric, higher values for $\dot{W}_{tot}$, η_{tot} and ε_{tot} are desirable, while a lower $\dot{C}_{sys}$ is also favorable. As shown in Fig. 3, at the upper bound of T_{LCZ}, all the considered performance parameters reach their lowest values. In contrast, at the lower bound of T_{LCZ}, these parameters attain the maximum values. This trade-off presents a conflicting situation, making it difficult to determine an optimal value of T_{LCZ} based solely on the parametric analysis. Figure 4 shows how ZT_m influences the overall system's performance characteristics and cost rate. As ZT_m rises from 0.2 to 1.6, $\dot{W}_{tot}$, η_{tot}, ε_{tot} and $\dot{C}_{sys}$ also increase. This occurs because a higher ZT_m enhances the TEG's power generation capacity, improving both energy and exergy efficiencies. However, this increase in power output is accompanied by a rise in TEG's purchase cost, which in turn raises $\dot{C}_{sys}$. At the upper end of ZT_m the values for power output, efficiencies, and system cost rate reach their peak, while at the lower end, they are minimized. This trade-off highlights a complex challenge in identifying an optimal ZT_m solely through parametric analysis, as each increase in ZT_m entails both performance gains and higher costs.

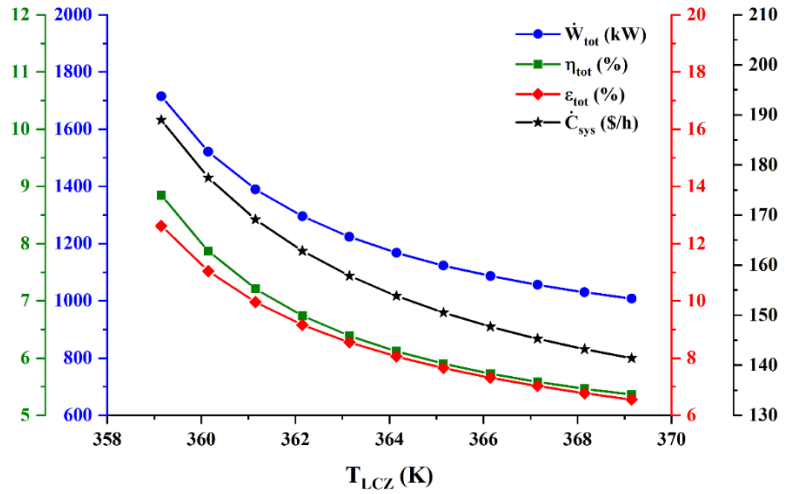

Fig. 3. The effect of T_{LCZ} on the performance of SGSP integrated power plant

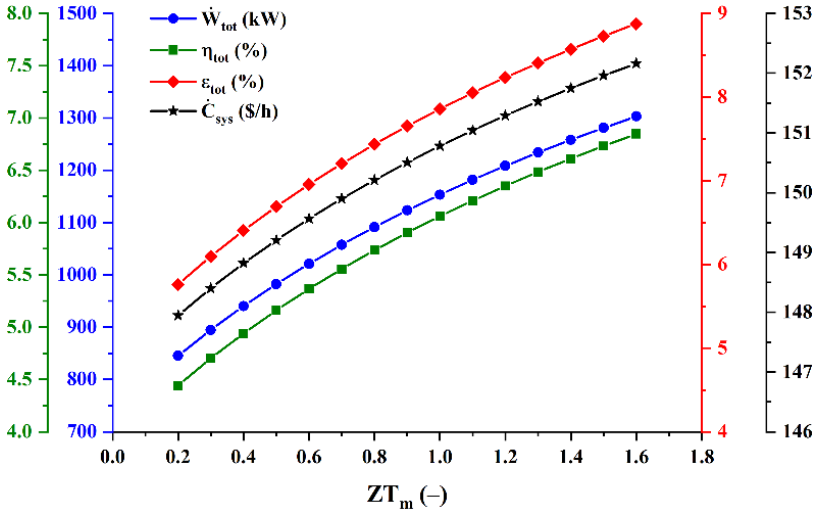

Fig. 4. The effect of ZT_m on the performance of SGSP integrated power plant.

Figure 5 shows how the main performance indices of the SGSP integrated power system vary with changes in T_7. An increase in T_7 enhances thermal performance but adversely impacts the economic performance of the system. It is observed that power output, energy efficiency, and exergy efficiency follow a similar pattern, showing a consistent slope. In contrast, the system cost rate exhibits a stepwise rise with a steeper slope. This indicates a trade-off: as the T_7 rises, power output, energy efficiency, and exergy efficiency improve, but the system cost rate also increases.

Figure 6 depicts the variation in the performance of the SGSP integrated power system as $\boldsymbol{T_{11}}$ increases from 300 K to 308 K. The RR-ORC power output falls as $\boldsymbol{T_{11}}$ rise, reducing total power output and resulting in decreased system efficiency. Conversely, the system cost rises, driven by increased exergy destruction costs within the condenser as the temperature rises. Unlike other operating parameters, $\boldsymbol{T_{11}}$ does not present a trade-off. At the lower limit of 300 K, power output, energy efficiency, and exergy efficiency reach their peak values, while the system cost rate is at its minimum. This indicates that a $\boldsymbol{T_{11}}$ of 300 K is optimal for operating the proposed system.

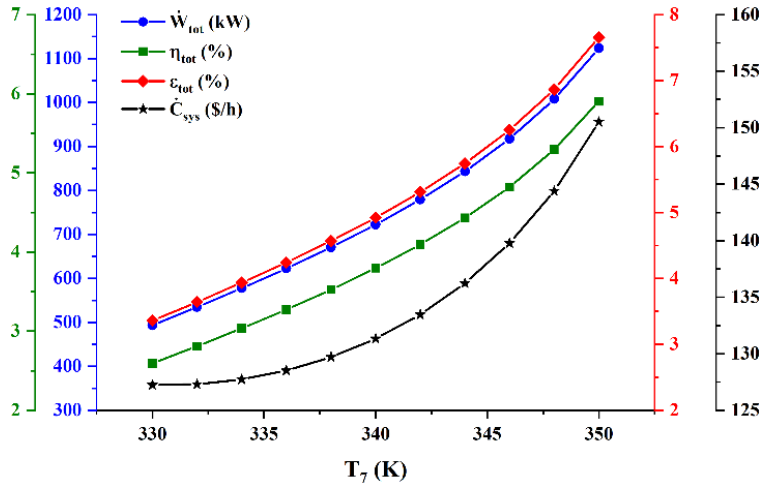

Fig. 5. The effect of T_7 on the performance of SGSP integrated power plant.

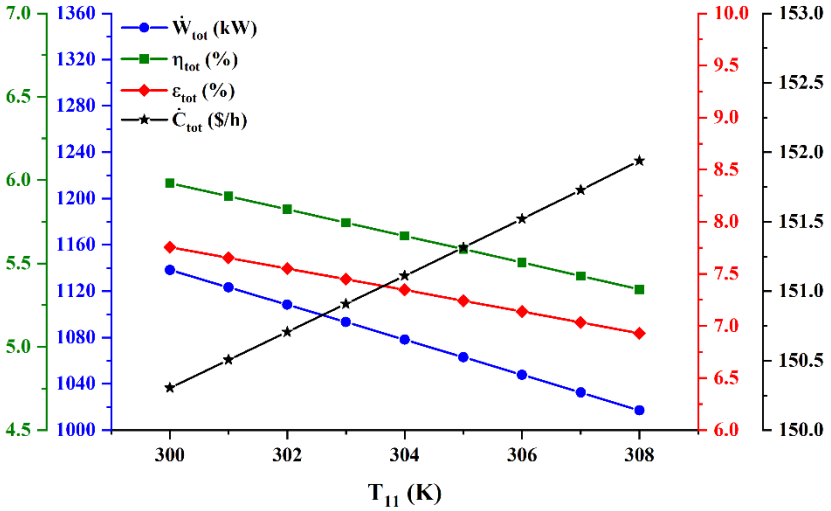

Fig. 6. The effect of T_{11} on the performance of the SGSP integrated power plant.

Figure 7 illustrates the variation in the performance of the power plant as $\dot{m}_r$ in the RR-ORC increases. As $\dot{m}_r$ rises from 10 kg/s to 50 kg/s, all these performance indices show a corresponding increase. This occurs because the higher mass flow rate of R123 enhances the power output of the RR-ORC, which, in turn, boosts the overall power output of the combined system. The energy and exergy efficiencies also improve due to the increased total power output. However, the system cost rate rises as well, driven by higher equipment purchase costs and exergy destruction costs within the RR-ORC components. A trade-off is observed here: while increased mass flow rates improve power output, energy efficiency, and exergy efficiency, they also lead to a higher system cost rate.

The parametric analysis reveals that, among the selected critical operating conditions, factors such as the low conductive zone, figure of merit, VT inlet temperature, and mass flow rate of R123 contribute to achieving a balance between thermal performance and system cost rate. Notably, the analysis indicates that setting the condenser temperature at its lower bound (300 K) is optimal, as it improves thermal performance while reducing the system cost rate. Consequently, to evaluate the optimum values of the remaining operating variables, multi-objective optimization is necessary, using these conditions as decision variables and targeting exergy efficiency and system cost rate as the objective functions.

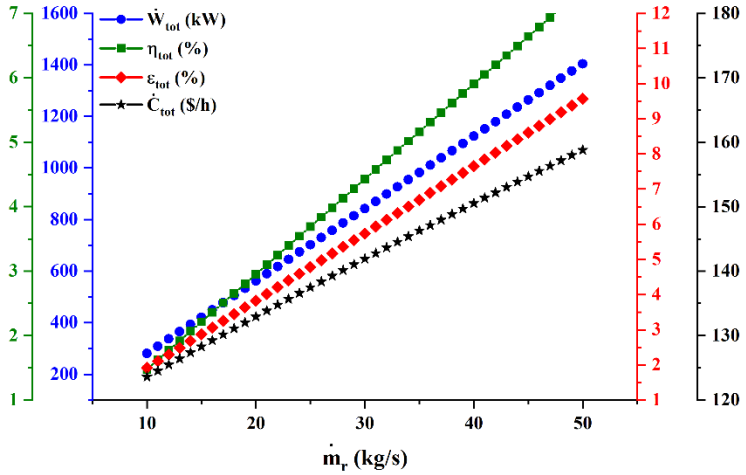

Fig. 7. The effect of $\dot{m}_r$ on the performance of SGSP integrated power plant.

4.3 Optimization results

Figure 8 presents the set of optimal parameters obtained from the multi-objective optimisation in the form of a Pareto front. As outlined earlier, this optimisation aims to enhance exergy efficiency while reducing system cost rate, using the low conductive zone, figure of merit, VG outlet temperature, and mass flow rate of R123 as decision variables. The TOPSIS method is used to find a single optimal solution from the Pareto front. This step is necessary because, while all solutions on the Pareto front are optimal, practical applications—such as optimizing a power plant—require a single, definitive solution that represents specific operating conditions. In the TOPSIS method, users assign weights to each objective function to indicate priority. For this study, an equal weight of 0.5 is assigned to both ε_{tot} and $\dot{C}_{sys}$ reflecting the balanced importance between the two objectives.

The multi-objective optimization yielded optimal decision variables and objective functions, as summarized in Tables 6 and 7.

Table 6. Optimal decision variables obtained from multi-objective optimization.

Parameters	Units	Values
T_{LCZ}	K	360.51
ZT_m	–	1.58
T_7	K	349.18
$\dot{m}_r$	kg/s	48.95

Table 7. Optimal objective function obtained from multi-objective optimization.

Parameters	Units	Values
ε_{tot}	%	14.36
$\dot{C}_{sys}$	$/h	182.94

The key decision variables include the lower convective zone temperature (T_{LCZ} = 360.51 K), figure of merit (ZT_m= 1.58), inlet temperature of the VT (T_7= 349.18 K), and mass flow rate of R123 ($\dot{m}_r$= 48.95 kg/s). These parameters ensure an optimal balance between thermodynamic performance and cost-effectiveness. The corresponding objective functions—total exergy efficiency (ε_{tot}= 14.36 %) and system cost rate ($\dot{C}_{sys}$ = 182.94 $/h).). In addition, under optimal conditions, the system delivers a power output of 1987 kW, with an energy efficiency of 10.3%.

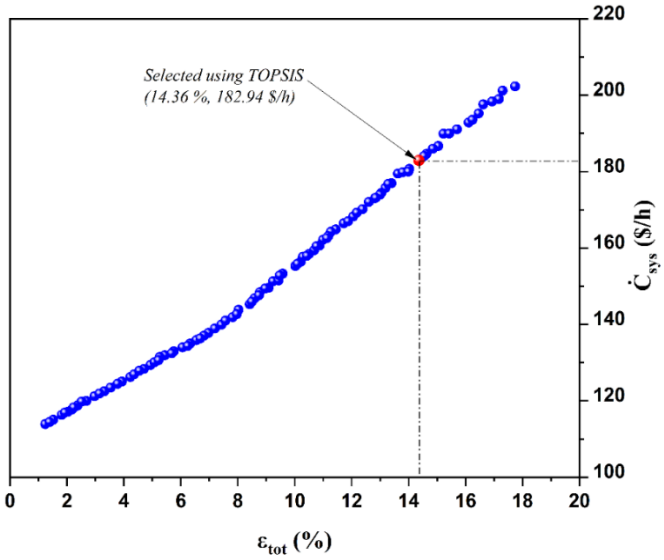

Fig. 8. Illustration of Pareto in objective space.

The improvement in the performance parameter of the system demonstrates that the proposed configuration achieves a favorable compromise between energy utilization and economic viability.

At optimal operating conditions, the total exergy destruction of the plant is found to be 11,343 kW. The contribution of each component to this total is depicted in Fig. 9. It is observed that the SGSP contributes 65.41% of the total exergy destruction, followed by the TEG with 30.81%, and the RR-ORC, which accounts for 3.78%. The VT contributes the most to exergy destruction within the RR-ORC components, followed by the VG and FH. The remaining components of the RR-ORC make a negligible contribution to the overall exergy destruction. The overall capital cost rate of the proposed plant is determined to be $116.14 $/h. Figure 10 illustrates the distribution of this cost among the subsystems. The SGSP contributes the largest share, accounting for 57.44% of total capital cost, followed by the TEG and RR-ORC subsystems, with respective shares of 27.42% and 15.14%. Within the RR-ORC subsystem, the VT component has the highest contribution at 11.58%, followed by the condenser (COND) at 1.45%. The remaining components of the RR-ORC make a negligible contribution to the overall capital cost rate of the integrated plant.

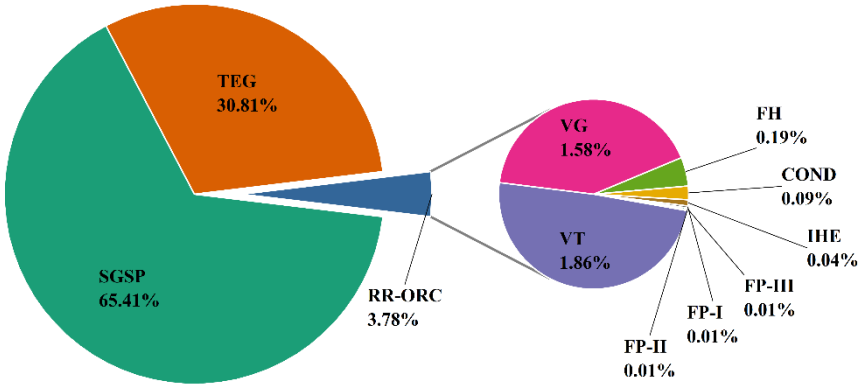

Fig. 9. Exergy destruction rate for each component at optimal operating condition.

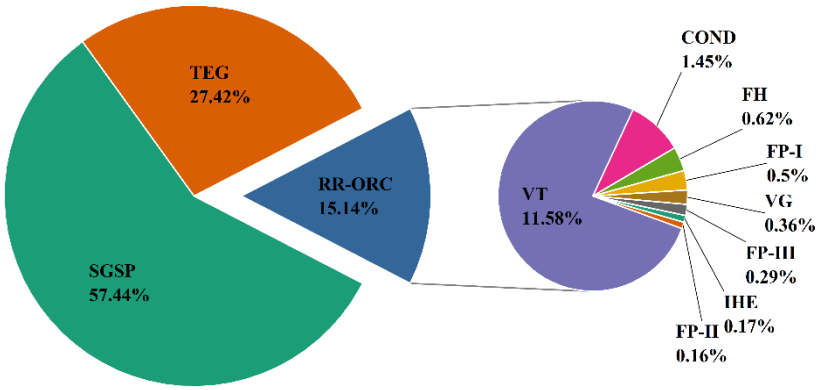

Fig. 10. Capital cost rate for each component at optimal operating condition.

Table 8 presents the economic analysis under these optimal conditions. The total investment cost amounts to $27,538,000, and the annual net cash flow amounts to $3,202,100. The simple payback period is estimated at 8.6 years, while the payback period, accounting for the time value of money, extends to 10.1 years, indicating reasonable financial feasibility for long-term implementation.

Table 8. Results of economic analysis at optimal operating condition.

Parameters	Values
Total investment cost	$27,538,000
Annual net cash flow	$3,202,100
Simple payback period	8.6 years
Payback period	10.1 years

Figure 11 illustrates the scattered distribution of decision variables corresponding to the Pareto front generated by the best run of NSGA-II. These distributions represent the population within the decision space for the four decision variables along the Pareto front. Figure 11(a) shows the scattered distribution of the VT inlet temperature, with optimal points distributed across the range of 338 to 350 K. This range is identified as the most suitable for achieving optimized system performance. The dispersed spread indicates that the VT inlet temperature plays a critical role in the trade-off between the objective functions, making it a key factor in multi-objective optimization. A similar pattern is observed in Fig. 11(b), which depicts the scattered distribution of the low conductive zone temperature. Optimal points are randomly distributed across a range of 359.15 K to 368 K, highlighting the sensitivity of this variable to the trade-off between objective functions. Figure 11(c) presents the scattered distribution of the figure of merit, where the population is clustered proximal to the upper bound. This suggests that increasing the figure of merit enhances exergy efficiency and reduces the system cost rate without introducing significant trade-offs. Finally, Fig. 11(d) illustrates the scattered distribution for the mass flow rate of R123. While most of the population is clustered near the upper bound, some points are randomly spread throughout the decision space, resembling outliers. This indicates that the mass flow rate of R123 is less sensitive concerning the trade-off between objective functions.

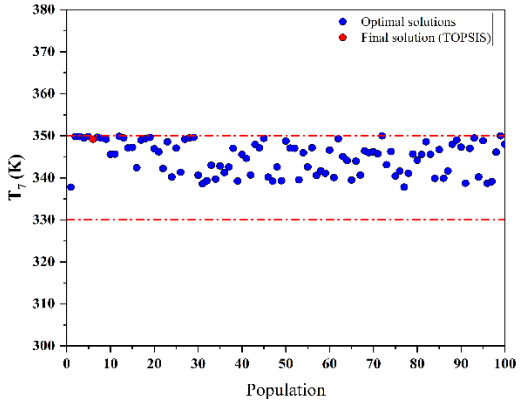

(a) VT inlet temperature

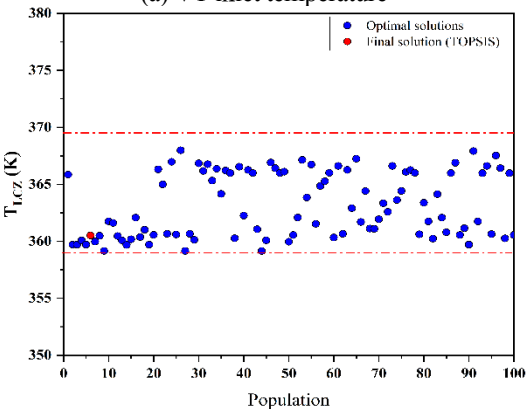

(b) Low conductive zone temperature

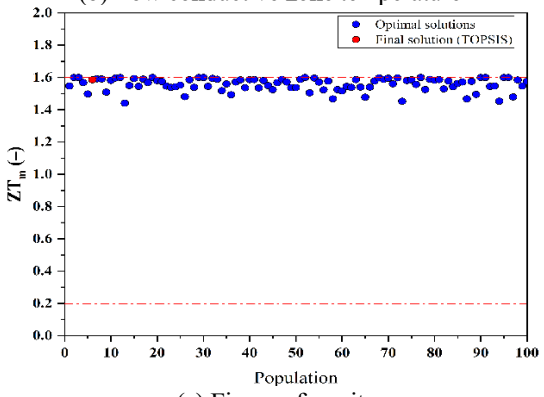

(c) Figure of merit

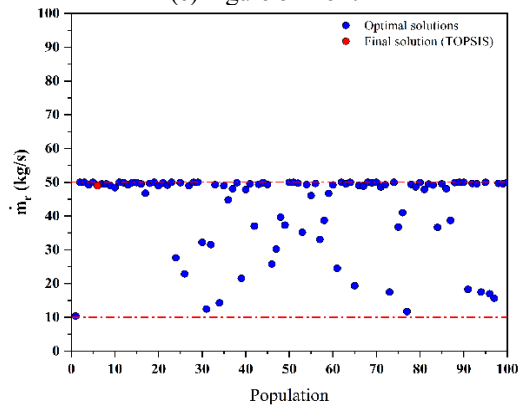

(d) Mass flow rate of R123

Fig. 11. Scattered distribution plots.

5. Conclusions

This study presents a solar pond-based combined power plant, integrating an RR-ORC with a thermoelectric generator to enhance power generation. Through 3E analyses, the performance and cost rate of the system were evaluated, revealing valuable insights into the optimization of its operation. The parametric analysis demonstrated how critical operating conditions such as low conductive zone temperature, figure of merit, VT inlet temperature, condenser temperature, and mass flow rate of R123 significantly influence the system's thermal performance and cost rate. Notably, a trade-off between improved power output, energy efficiency, and reduced system cost rate was observed, with specific optimal conditions identified for each parameter. The multi-objective optimization using NSGA-II and TOPSIS methods provided an optimal solution that balances the objective functions. The results indicate that under optimal operating conditions, the system delivers a power output of 1987 kW, with energy and exergy efficiencies of 10.3% and 14.36%, respectively, and a system cost rate of $182.94 per hour. These results underscore the importance of careful optimization of operating parameters, especially the VT inlet temperature and low conductive zone temperature, to achieve the best performance.

The proposed solar pond-based combined power plant demonstrates promising potential for efficient low-temperature power generation. The findings highlight the importance of a balanced approach between thermal performance and economic viability, offering insights for future developments in renewable energy systems. Further research into refining the optimization process and exploring other working fluids may further improve system performance and cost-effectiveness, contributing to the sustainability of solar pond technologies in real-world applications.

References

[1] Kasaeian A, Sharifi S, Yan WM. Novel achievements in the development of solar ponds: A review. Solar Energy 2018;174:189–206. https://doi.org/10.1016/j.solener.2018.09.010.

[2] Bernad F, Casas S, Gibert O, Akbarzadeh A, Cortina JL, Valderrama C. Salinity gradient solar pond: Validation and simulation model. Solar Energy 2013;98:366–74. https://doi.org/10.1016/j.solener.2013.10.004.

[3] Tawalbeh M, Javed RMN, Al-Othman A, Almomani F. Salinity gradient solar ponds hybrid systems for power generation and water desalination. Energy Convers Manag 2023;289:117180. https://doi.org/10.1016/J.ENCONMAN.2023.117180.

[4] Khalilian M. Assessment of the overall energy and exergy efficiencies of the salinity gradient solar pond with shading effect. Solar Energy 2017;158:311–20. https://doi.org/10.1016/j.solener.2017.09.059.

[5] El Mansouri A, Hasnaoui M, Amahmid A, Dahani Y. Transient theoretical model for the assessment of three heat exchanger designs in a large-scale salt gradient solar pond: Energy and exergy analysis. Energy Convers Manag 2018;167:45–62. https://doi.org/10.1016/j.enconman.2018.04.087.

[6] Babaei HR, Khoshvaght-Aliabadi M, Mazloumi SH. Analysis of serpentine coil with alternating flattened axis: An insight into performance enhancement of solar ponds. Solar Energy 2021;217:292–307. https://doi.org/10.1016/j.solener.2021.02.017.

[7] Dehghan AA, Movahedi A, Mazidi M. Experimental investigation of energy and exergy performance of square and circular solar ponds. Solar Energy 2013;97:273–84. https://doi.org/10.1016/j.solener.2013.08.013.

[8] Njoku HO, Agashi BE, Onyegegbu SO. A numerical study to predict the energy and exergy performances of a salinity gradient solar pond with thermal extraction. Solar Energy 2017;157:744–61. https://doi.org/10.1016/j.solener.2017.08.079.

[9] Faqeha H, Bawahab M, Vermont D, Date A, Akbarzadeh A. Setting up salinity gradient

in an experimental solar pond (SGSP). Energy Procedia, vol. 156, Elsevier Ltd; 2019, p. 115–21. https://doi.org/10.1016/j.egypro.2018.11.114.

[10] Ziapour BM, Saadat M, Palideh V, Afzal S. Power generation enhancement in a salinity-gradient solar pond power plant using thermoelectric generator. Energy Convers Manag 2017;136:283–93. https://doi.org/10.1016/J.ENCONMAN.2017.01.031.

[11] Damarseckin S, Atiz A, Karakilcik M. Solar pond integrated with parabolic trough solar collector for producing electricity and hydrogen. Int J Hydrogen Energy 2024;52:115–26. https://doi.org/10.1016/J.IJHYDENE.2023.02.087.

[12] Musharavati F, Khanmohammadi S, Nondy J, Gogoi TK. Proposal of a new low-temperature thermodynamic cycle : 3E analysis and optimization of a solar pond integrated with fuel cell and thermoelectric generator. J Clean Prod 2022;331:129908. https://doi.org/10.1016/j.jclepro.2021.129908.

[13] Zeynali A, Akbari A, Khalilian M. Investigation of the performance of modified organic Rankine cycles (ORCs) and modified trilateral flash cycles (TFCs) assisted by a solar pond. Solar Energy 2019;182:361–81. https://doi.org/10.1016/j.solener.2019.03.001.

[14] Mosaffa AH, Farshi LG. Thermodynamic feasibility evaluation of an innovative salinity gradient solar ponds-based ORC using a zeotropic mixture as working fluid and LNG cold energy. Appl Therm Eng 2021;186:116488. https://doi.org/10.1016/j.applthermaleng.2020.116488.

[15] Masoud Parsa S, Majidniya M, Alawee WH, Dhahad HA, Muhammad Ali H, Afrand M, et al. Thermodynamic, economic, and sensitivity analysis of salt gradient solar pond (SGSP) integrated with a low-temperature multi effect desalination (MED): Case study, Iran. Sustainable Energy Technologies and Assessments 2021;47:101478. https://doi.org/10.1016/J.SETA.2021.101478.

[16] Manzoor K, Khan SJ, Jamal Y, Shahzad MA. Heat extraction and brine management from salinity gradient solar pond and membrane distillation. Chemical Engineering Research and Design 2017;118:226–37. https://doi.org/10.1016/J.CHERD.2016.12.017.

[17] El Mansouri A, Hasnaoui M, Amahmid A, Hasnaoui S. Feasibility analysis of reverse osmosis desalination driven by a solar pond in Mediterranean and semi-arid climates. Energy Convers Manag 2020;221:113190. https://doi.org/10.1016/J.ENCONMAN.2020.113190.

[18] Li J, Dhahad HA, Anqi AE, Rajhi AA. Thermo-economic investigation on the hydrogen production through the stored solar energy in a salinity gradient solar pond: A comparative study by employing APC and ORC with zeotropic mixture. Int J Hydrogen Energy 2022;47:7600–23. https://doi.org/10.1016/J.IJHYDENE.2021.12.102.

[19] Zoghi M, Hosseinzadeh N, Gharaie S, Zare A. Energy and exergy-economic performance comparison of wind, solar pond, and ocean thermal energy conversion systems for green hydrogen production. Int J Hydrogen Energy 2024. https://doi.org/10.1016/J.IJHYDENE.2024.06.183.

[20] Nondy J, Gogoi TK. Exergoeconomic investigation and multi-objective optimization of different ORC configurations for waste heat recovery: A comparative study. Energy Convers Manag 2021;245:114593. https://doi.org/10.1016/J.ENCONMAN.2021.114593.

[21] Ziapour BM, Shokrnia M, Naseri M. Comparatively study between single-phase and two-phase modes of energy extraction in a salinity-gradient solar pond power plant. Energy 2016;111:126–36. https://doi.org/10.1016/j.energy.2016.05.114.

[22] Rostamzadeh H, Nourani P. Investigating potential benefits of a salinity gradient solar

pond for ejector refrigeration cycle coupled with a thermoelectric generator. Energy 2019;172:675–90. https://doi.org/10.1016/j.energy.2019.01.167.

[23] Anvari S, Jafarmadar S, Khalilarya S. Proposal of a combined heat and power plant hybridized with regeneration organic Rankine cycle: Energy-Exergy evaluation. Energy Convers Manag 2016;122:357–65. https://doi.org/10.1016/j.enconman.2016.06.002.

[24] Aliahmadi M, Moosavi A, Sadrhosseini H. Multi-objective optimization of regenerative ORC system integrated with thermoelectric generators for low-temperature waste heat recovery. Energy Reports 2021;7:300–13. https://doi.org/10.1016/j.egyr.2020.12.035.

[25] Guo Q, Khanmohammadi S. Comparison of exergy and exergy economic evaluation of different geothermal cogeneration systems for optimal waste energy recovery. Chemosphere 2023;339:139586. https://doi.org/10.1016/J.CHEMOSPHERE.2023.139586.

[26] Nondy J. 4E analyses of a micro-CCHP system with a polymer exchange membrane fuel cell and an absorption cooling system in summer and winter modes. Int J Hydrogen Energy 2024;52:886–904. https://doi.org/10.1016/J.IJHYDENE.2023.06.220.

[27] Goswami A, Gogoi TK. Design of components of a steam power plant and its exergoeconomic performance analysis. Thermal Science and Engineering Progress 2024;47:102276. https://doi.org/10.1016/J.TSEP.2023.102276.

[28] Valero A, Serra L, Uche J. Fundamentals of exergy cost accounting and thermoeconomics. Part II: Applications. Journal of Energy Resources Technology, Transactions of the ASME 2006;128:9–15. https://doi.org/10.1115/1.2134731.

[29] Bejan, Adrian, George Tsatsaronis and MJMoran. Thermal design and optimization. New York: John Wiley & Sons; 1995.

[30] Nondy J, Gogoi TK. A comparative study of metaheuristic techniques for the thermoenvironomic optimization of a gas turbine-based benchmark combined heat and power system. J Energy Resour Technol 2020;143:062104. https://doi.org/10.1115/1.4048534.

[31] Mehrpooya M, Sharifzadeh MMM, Zonouz MJ, Rosen MA. Cost and economic potential analysis of a cascading power cycle with liquefied natural gas regasification. Energy Convers Manag 2018;156:68–83. https://doi.org/10.1016/J.ENCONMAN.2017.10.100.

[32] Khanmohammadi S, Azimian AR. Exergoeconomic Evaluation of a Two-Pressure Level Fired Combined-Cycle Power Plant. Journal of Energy Engineering 2015;141:04014014. https://doi.org/10.1061/(asce)ey.1943-7897.0000152.

[33] Mehrpooya M, Ansarinasab H, Moftakhari Sharifzadeh MM, Rosen MA. Process development and exergy cost sensitivity analysis of a hybrid molten carbonate fuel cell power plant and carbon dioxide capturing process. J Power Sources 2017;364:299–315. https://doi.org/10.1016/J.JPOWSOUR.2017.08.024.

[34] Zarei A, Akhavan S, Rabiee MB, Elahi S. Energy, exergy and economic analysis of a novel solar driven CCHP system powered by organic Rankine cycle and photovoltaic thermal collector. Appl Therm Eng 2021;194:117091. https://doi.org/10.1016/j.applthermaleng.2021.117091.

[35] Esmaeilion F, Soltani M, Hoseinzadeh S, Sohani A, Nathwani J. Benefits of an innovative polygeneration system integrated with salinity gradient solar pond and desalination unit. Desalination 2023;564:116803. https://doi.org/10.1016/J.DESAL.2023.116803.

[36] Bellos E, Pavlovic S, Stefanovic V, Tzivanidis C, Nakomcic-Smaradgakis BB. Parametric analysis and yearly performance of a trigeneration system driven by solar-dish collectors. Int J Energy Res 2019;43:1534–46. https://doi.org/10.1002/ER.4380.

[37] Habibollahzade A, Houshfar E, Ashjaee M, Gholamian E, Behzadi A. Enhanced performance and reduced payback period of a low grade geothermal-based ORC through employing two TEGs. Energy Equipment and Systems 2019;7:23–39. https://doi.org/10.22059/EES.2019.34611.

[38] Deb K. Multi-objective optimization. In: Burke E, Kendall G, editors. Search Methodologies: Introductory Tutorials in Optimization and Decision Support Techniques, Second Edition, Springer, Boston, MA.; 2014, p. 403–50. https://doi.org/10.1007/978-1-4614-6940-7_15.

[39] Dincer I, Rosen MA, Ahmadi P. Optimization of Energy Systems. Chichester, UK: John Wiley & Sons, Ltd; 2017. https://doi.org/10.1002/9781118894484.

[40] Anvari S, Taghavifar H, Parvishi A. Thermo- economical consideration of Regenerative organic Rankine cycle coupling with the absorption chiller systems incorporated in the trigeneration system. Energy Convers Manag 2017;148:317–29. https://doi.org/10.1016/j.enconman.2017.05.077.

[41] Nondy J, Gogoi TK. A Comparative Study of Metaheuristic Techniques for the Thermoenvironomic Optimization of a Gas Turbine-Based Benchmark Combined Heat and Power System. J Energy Resour Technol 2020;143:062104. https://doi.org/10.1115/1.4048534.

[42] Heidarnejad P, Genceli H, Asker M, Khanmohammadi S. A comprehensive approach for optimizing a biomass assisted geothermal power plant with freshwater production: Techno-economic and environmental evaluation. Energy Convers Manag 2020;226:113514. https://doi.org/10.1016/j.enconman.2020.113514.

[43] Çelikbilek Y, Tüysüz F. An in-depth review of theory of the TOPSIS method: An experimental analysis. Journal of Management Analytics 2020;7:281–300. https://doi.org/10.1080/23270012.2020.1748528.

[44] Alao MA, Ayodele TR, Ogunjuyigbe ASO, Popoola OM. Multi-criteria decision based waste to energy technology selection using entropy-weighted TOPSIS technique: The case study of Lagos, Nigeria. Energy 2020;201:117675. https://doi.org/10.1016/j.energy.2020.117675.

[45] Nondy J, Gogoi TK. Exergoeconomic investigation and multi-objective optimization of different ORC configurations for waste heat recovery: A comparative study. Energy Convers Manag 2021;245:114593. https://doi.org/10.1016/J.ENCONMAN.2021.114593.

[46] Jingwen Huang. Combining entropy weight and TOPSIS method for information system selection. 2008 IEEE Conference on Cybernetics and Intelligent Systems, Chengdu, China: IEEE; 2008, p. 1281–4. https://doi.org/10.1109/ICCIS.2008.4670971.

[47] Tsilingiris PT. Computer simulation modelling, thermal performance and design optimisation for solar ponds in Greece. Solar and Wind Technology 1988;5:645–52. https://doi.org/10.1016/0741-983X(88)90062-8.

[48] Ziapour BM, Shokrnia M, Naseri M. Comparatively study between single-phase and two-phase modes of energy extraction in a salinity-gradient solar pond power plant. Energy 2016;111:126–36. https://doi.org/10.1016/J.ENERGY.2016.05.114.

[49] Safarian S, Aramoun F. Energy and exergy assessments of modified Organic Rankine Cycles (ORCs). Energy Reports 2015;1:1–7. https://doi.org/10.1016/j.egyr.2014.10.003.

[50] Safarian S, Aramoun F. Energy and exergy assessments of modified Organic Rankine Cycles (ORCs). Energy Reports 2015;1:1–7. https://doi.org/10.1016/j.egyr.2014.10.003.